Experimental Neurology 283 (2016) 165–178

Contents lists available at ScienceDirect

Experimental Neurology

journal homepage: www.elsevier.com/locate/yexnr

Research Paper

Ligand-mediated Galectin-1 endocytosis prevents intraneural H_2O_2 production promoting F-actin dynamics reactivation and axonal re-growth

Héctor R. Quintá [a], Carlos Wilson [b], Ada G. Blidner [c], Christian González-Billault [b], Laura A. Pasquini [a], Gabriel A. Rabinovich [c,d], Juana M. Pasquini [a,*]

[a] Departamento de Química Biológica, Instituto de Química y Físico Química Biológica, Universidad de Buenos Aires, Buenos Aires C1113AAD, Argentina
[b] Laboratory of Cell and Neuronal Dymanics, Faculty of Sciences, Universidad de Chile. Center for Geroscience, Brain Health and Metabolism, Santiago, Chile. The Buck Institute for Research on Aging, Novato, USA
[c] Laboratorio de Inmunopatología, Instituto de Biología y Medicina Experimental (IBYME), Consejo Nacional de Investigaciones Científicas y Técnicas (CONICET). Buenos Aires C1428, Argentina
[d] Facultad de Ciencias Exactas y Naturales, Universidad de Buenos Aires, Buenos Aires, C1428, Argentina

ARTICLE INFO

Article history:
Received 29 February 2016
Received in revised form 8 May 2016
Accepted 9 June 2016
Available online 11 June 2016

Keywords:
Axonal growth
Filamentous actin
Hydrogen peroxide
Galectin-1
PlexinA4
Semaphorin3A
Spinal cord injury

ABSTRACT

Axonal growth cone collapse following spinal cord injury (SCI) is promoted by semaphorin3A (Sema3A) signaling via PlexinA4 surface receptor. This interaction triggers intracellular signaling events leading to increased hydrogen peroxide levels which in turn promote filamentous actin (F-actin) destabilization and subsequent inhibition of axonal re-growth. In the current study, we demonstrated that treatment with galectin-1 (Gal-1), in its dimeric form, promotes a decrease in hydrogen peroxide (H_2O_2) levels and F-actin repolimerization in the growth cone and in the filopodium of neuron surfaces. This effect was dependent on the carbohydrate recognition activity of Gal-1, as it was prevented using a Gal-1 mutant lacking carbohydrate-binding activity. Furthermore, Gal-1 promoted its own active ligand-mediated endocytosis together with the PlexinA4 receptor, through mechanisms involving complex branched N-glycans. In summary, our results suggest that Gal-1, mainly in its dimeric form, promotes re-activation of actin cytoskeleton dynamics via internalization of the PlexinA4/Gal-1 complex. This mechanism could explain, at least in part, critical events in axonal regeneration including the full axonal re-growth process, *de novo* formation of synapse clustering, axonal re-myelination and functional recovery of coordinated locomotor activities in an *in vivo* acute and chronic SCI model.
Significance statement: Axonal regeneration is a response of injured nerve cells critical for nerve repair in human spinal cord injury. Understanding the molecular mechanisms controlling nerve repair by Galectin-1, may be critical for therapeutic intervention. Our results show that Galectin-1; in its dimeric form, interferes with hydrogen peroxide production triggered by Semaphorin3A. The high levels of this reactive oxygen species (ROS) seem to be the main factor preventing axonal regeneration due to promotion of actin depolymerization at the axonal growth cone. Thus, Galectin-1 administration emerges as a novel therapeutic modality for promoting nerve repair and preventing axonal loss.

© 2016 Elsevier Inc. All rights reserved.

1. Introduction

Although underappreciated for many years, emerging observations suggest essential roles for glycan-binding proteins and their corresponding glycosylated ligands in different central nervous system (CNS) pathologies (Rabinovich and Croci, 2012; Mendez-Huergo et al., 2014). In previous studies, we reported the functional recovery of mice with spinal cord injury (SCI) following local treatment with galectin-1 (Gal-1), a highly conserved glycan-binding protein, through mechanisms involving interruption of Semaphorin3A (Sema3A)-driven inhibitory signals (Quinta et al., 2014b). We found that Gal-1 binds to the Neuropilin-1 (NRP-1)/PlexinA4 receptor complex on the surface of injured neurons through a glycan-dependent mechanism, promoting axonal regeneration. However, the molecular mechanism through which Gal-1 association with NRP-1/PlexinA4 promotes axonal re-growth remains uncertain.

It is well known that Sema3A, a chemo-repulsive axonal guidance molecule, induces growth cone collapse after SCI (Takahashi et al., 1999). This protein is secreted by meningeal fibroblasts spreading out at the lesion site (Pasterkamp et al., 1999), where it binds to NRP-1/PlexinA4 surface receptor in the injured axonal tracts (Tamagnone et al., 1999; Pasterkamp and Verhaagen, 2001; De Winter et al., 2002a; De Winter et al., 2002b). This interaction, leads to intracellular signaling events that raise MICAL activity,

* Corresponding author.
E-mail address: jpasquin@qb.ffyb.uba.ar (J.M. Pasquini).

http://dx.doi.org/10.1016/j.expneurol.2016.06.009
0014-4886/© 2016 Elsevier Inc. All rights reserved.

thus promoting an increase in intra-axonal hydrogen peroxide (H_2O_2) production, which in turn oxidizes F-actin at methionine residues, resulting in F-actin destabilization. The whole process generates growth cone collapse (sharp decrease in F-actin length and bundling) and inhibition of axonal re-growth (Hung and Terman, 2011; Giridharan and Caplan, 2014). Moreover, neuronal H_2O_2 production over physiological levels is closely associated with axonal growth failure (Hung et al., 2010; Hung et al., 2011; Morinaka et al., 2011), supporting a link between inhibition of axonal regeneration and production of reactive oxygen species (ROS).

From a biochemical viewpoint, Gal-1 is an endogenous homodimeric lectin composed of subunits of 14.5 kDa that binds to glycosylated receptors displaying multiple units of the common disaccharide (Galβ1–4)GlcNAc; LacNac) on both *N*- and *O*-glycans (Rabinovich and Croci, 2012). Within the CNS, injection of Gal-1 following SCI, binds to the NRP-1/PlexinA4 complex, promoting axonal regeneration and recovery of locomotor activities (Quinta et al., 2014b). However, in spite of considerable progress the molecular mechanisms underlying this neuro-regenerative effect remain uncertain.

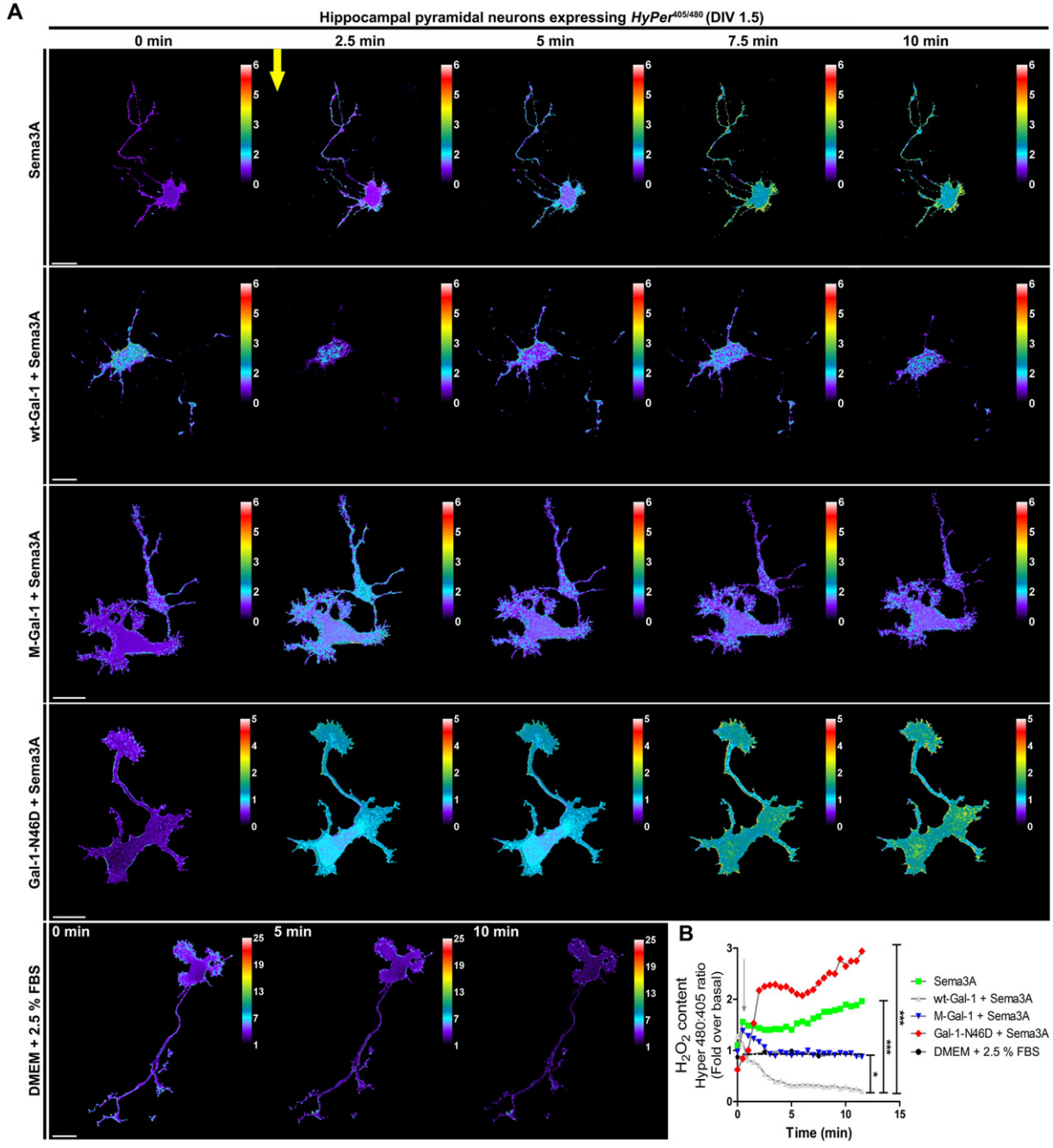

Fig. 1. Real time measurement of H_2O_2 production in hippocampal pyramidal neurons. (A) H_2O_2 content evaluated by confocal time-lapse acquisition of representative HyPer transfected neurons. The experimental conditions were: 300 μg/ml of Sema3A (first line); 280 μg/ml of wt-Gal-1 (15 min of pre-incubation) + 300 μg/ml of Sema3A (second line); 280 μg/ml of M-Gal-1 (15 min of pre-incubation) + 300 μg/ml of Sema3A (third line); 280 μg/ml of Gal-1-N46D (15 min of pre-incubation) + 300 μg/ml of Sema3A (fourth line). The yellow line indicates Sema3A addition. Basal H_2O_2 content control evaluated in HyPer transfected neurons (fifth line). In the right corner of each picture, a calibration bar is shown (0–255 colors) normalized for each condition. Scale bar, 20 μm. (B) Graphical analysis shows a quantification of H_2O_2 content 480:405 ratio (fold over basal). The gray arrow in the bar graph indicates Sema3A addition. Values represent the mean of three independent experiments (n = 5 transfected cells analyzed per condition). $^{***}P < 0.05$, $^{*}P < 0.05$ using one-way ANOVA followed by Dunn's multiple comparison tests.

Therefore, to determine whether wild-type recombinant Gal-1 in its dimeric conformation (wt-Gal-1) could reactivate actin dynamics via N-glycan recognition, we evaluated in real time the effect of Gals-1 *vs* Sema3A on H_2O_2 production in pyramidal neurons using a HyPer biosensor coupled to quantitative confocal video microscopy (Belousov et al., 2006; Cheng et al., 2014). We demonstrate that interactions between dimeric Gal-1 and NRP-1/PlexinA4 receptor leads to active internalization of the complex through an N-glycan-dependent mechanism, leading to decrease in H_2O_2 levels, even in the presence of Sema3A. The whole process promoted the reactivation of actin cytoskeleton dynamics in the growth cone as well as in the filopodia of neuronal surfaces. In addition, in an *in vivo* SCI model (acute and chronic), we found after wt-Gal-1 treatment, an internalization of Gal-1/PlexinA4 complex, full axonal regrowth, *de novo* formation of synapse clustering (synaptic vesicles accumulation), axonal re-myelination and functional recovery of coordinated locomotor activities. Our data unveil the molecular basis of the antagonic effects of Gal-1 and Sema3A signaling on NRP1/PlexinA4 complex and its functional consequences in neuro-regeneration.

2. Materials and methods

2.1. Primary culture of hippocampal pyramidal neurons

Dissociated hippocampal pyramidal neurons were isolated according to Kaech and Banker, 2006 (Kaech and Banker, 2006) from embryonic day-18.5 Sprague-Dawley rat embryos (provided by the animal

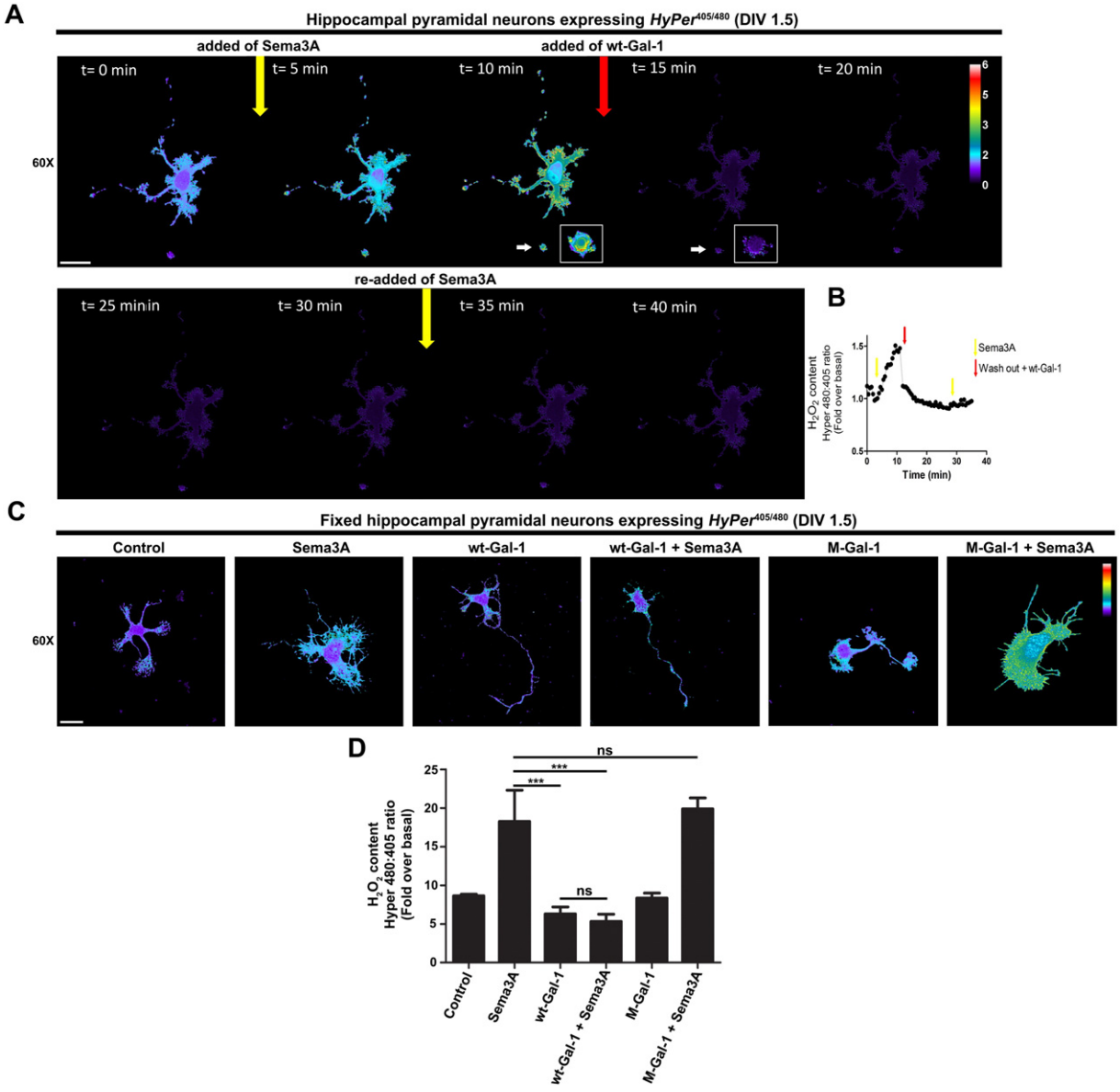

Fig. 2. Changes in H_2O_2 production by sequential addition of Sema3A and wt-Gal-1. (A) Dynamic H_2O_2 content evaluated by confocal time-lapse acquisition of representative HyPer transfected neurons. First, post-set H_2O_2 basal content, the neurons were treated with 300 μg/ml of Sema3A (yellow arrow point added), followed by a washout and addition of 280 μg/ml of wt-Gal-1 (red arrow) and final re-exposure to Sema3A. White arrows show H_2O_2 content at varicosities (white frames insets) pre- and post-wt-Gal-1 treatment. In the right corner a calibration bar is shown (0–255 colors). Scale bar, 20 μm. (B) Graphical analysis shows a quantification of H_2O_2 dynamic content 480:405 ratio (fold over basal). Values represent the mean of three independent experiments (n = 4 transfected cells analyzed). (C) Hyper-transfected neurons were incubated over 24 h with: 300 μg/ml of Sema3A; 280 μg/ml of wt-Gal-1; 300 μg/ml of Sema3A + 280 μg/ml of wt-Gal-1; 280 μg/ml of M-Gal-1; 300 μg/ml of Sema3A + 280 μg/ml of M-Gal-1. Basal H_2O_2 control content was evaluated in HyPer transfected neurons. In the right corner, a Calibration bar is shown (0–255 colors). Scale bar, 20 μm. (D) Bar graph shows a quantification of H_2O_2 content 480:405 ratio (fold over basal). Values represent the mean ± S.D. of three independent experiments (n = 10 transfected cells analyzed per condition). ***$P < 0.001$ and NS = not significant using one-way ANOVA followed by Tukey's tests.

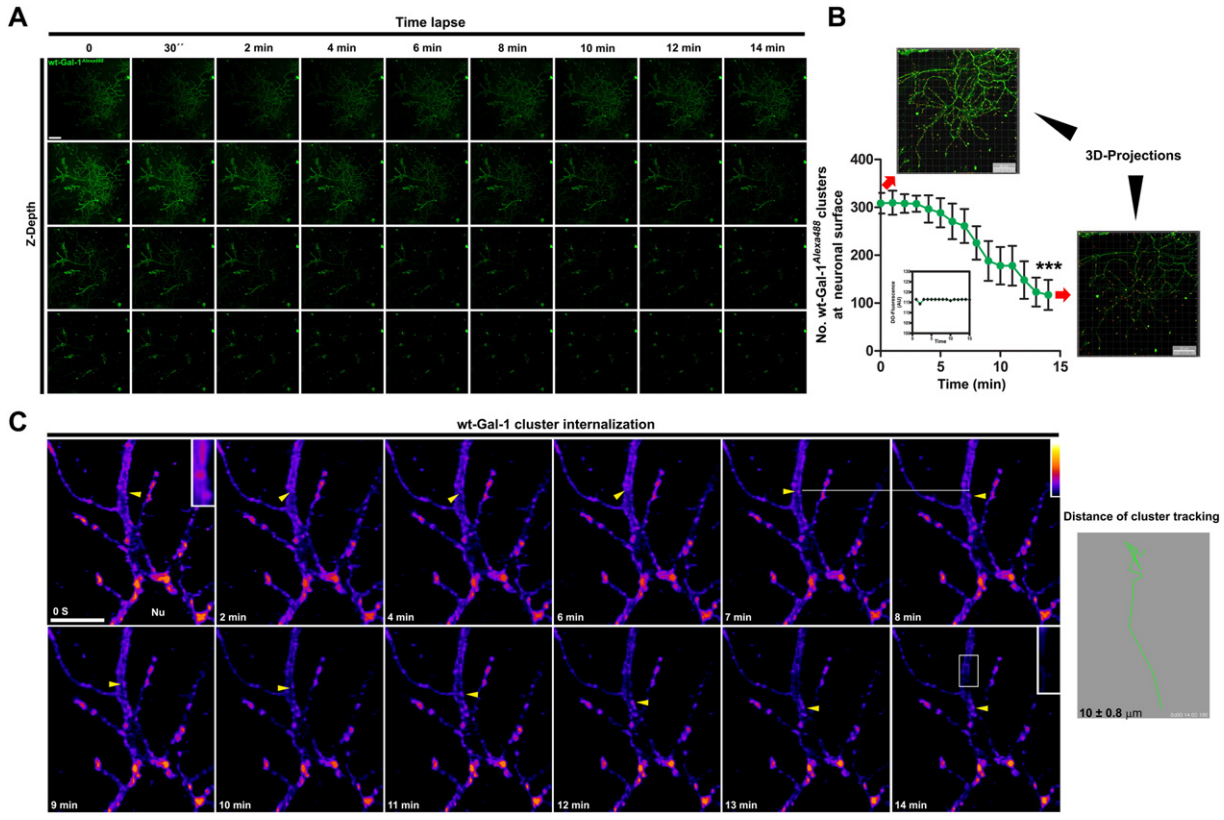

Fig. 3. Internalization of wild-type Gal-1 by neurons. (A) 4D confocal representative images showing the uptake of wt-Gal-1^{Alexa488} (280 μg/ml) by neurons. Scale bar, 50 μm. (B) Graphical analysis shows a quantification of the number of wt-Gal-1^{Alexa488} clusters at neuronal surface each 30 s during 15 min. Inset graph shows the fluorophore lifetime control. The representative 3D-projections were developed using Imaris 3D software, showing at time 0 s+ and time 14 min, the clustering (red dots) at the neuronal surface. Values represent the mean ± S.D. of 8 independent neurons analyzed. $^{***}P = 0.0003$ using one-way ANOVA followed by Tukey's tests. (C) Representative tracking of wt-Gal-1^{Alexa488} cluster from neuronal surface toward inside the axon. Yellow arrowhead point the localization of cluster in each time, starting at the neuronal surface (0 s picture inset) and ending inside the axon (14 min picture inset). Nu = nucleus. In the right corner, a calibration bar is shown (0–255 colors). Scale bar, 10 μm. Right picture shows a quantification of cluster trajectory.

facility of the Faculty of Medicine, University of Chile) and from post-natal-day-1 *Mgat5*$^{-/-}$ mice (provided by Jackson Lab). The isolated hippocampal cells were transiently maintained in Hanks' balanced salt solution. Briefly, hippocampal cells were digested with 0.25% trypsin-EDTA (Gibco-25200-056) for 24 min at 37 °C, followed by exposure to DMEM with 10% FBS and 10% F12. Dissociated neurons were plated onto a 1 mg/ml of poly-L-lysine pre-coated coverslips of 25 mm in culture dishes of 35 mm, and incubated at 37 °C in DMEM with 10% FBS and 10% F12 in a humidified 5% CO_2 atmosphere. Cultures were enriched for neurons by removing the plating medium after 2 h and replacing it with Neurobasal medium (Gibco-21103-049) supplemented with 2% B27 and 2 mM L-glutamine. Animal care and experimental procedures were carried out according to the guidelines of the Experimental Animal Care Committee of the School of Pharmacy and Biochemistry at the University of Buenos Aires, Argentina and by the Ethical Committee of the Faculty of Sciences, University of Chile.

2.2. Transfection with coding biosensor vector

The pyramidal hippocampal neurons were transfected with:

- HyPer biosensor (Evrogen, Moscow, Russia), a ratiometric sensor which detects local H_2O_2 production (Belousov et al., 2006).
- Lifeact-GFP or -Ruby biosensor (kindly provided by J. Bamburg), which allows real-time visualization of actin polymerization (Riedl et al., 2008).

Briefly, 200,000 cells/coverslip (25 mm) were transfected immediately after plating in the case of HyPer biosensor, and 18 h after plating in the case of Lifeact-GFP or -Ruby biosensor. Transfection was carried out using 2 μg cDNA and 5 μl Lipofectamine 2000 in Optimem medium, according to the manufacturer's instructions. After 2 h, Optimem

Fig. 4. Ligand-mediated endocytosis triggered by Gal-1 interaction with branched complex N-glycans. (A) Representative Z-projection of time lapse confocal images taken from neurons, treated with FR-D plus vehicle or wt-Gal-1 (280 μg/ml). The images were shown in spectrum graph generated with the Lut function of Fiji image processing software. In the right corner, a calibration bar is shown (0–255 colors). Inset in left panel shows the analyzed axon (black arrow). Right panel magnification of segments indicated by white arrows (1, 2 and 3) show the internalization of FR-D. Black arrowheads indicate FR-D in the process of internalization whereas white arrowheads indicate FR-D already internalized. Scale bar, 10 μm. Right bar graph shows a quantitative analysis of FR-D internalization. Values represent the mean ± S.D. of three independent experiments (n = 7 cells analyzed per condition). $^{***}P < 0.05$ using two-way ANOVA followed by Bonferroni's Multiple Comparison Test. (B) Lectin blot analysis of NRP-1 from wild type neurons. Binding of biotinylated PHA-L and biotinylated Gal-1 to immunoprecipitated NRP-1. Control of streptavidin alone ruled out non-specific lectin binding. (C) Representative Z-projection confocal images taken from neurons lacking the *Mgat5* glycosyltransferase treated with FR-D plus vehicle or wt-Gal-1 (280 μg/ml). Inset in each panel shows the analyzed axon (black arrow). Scale bar, 10 μm. (D) Triple staining, performed on the same neurons that were treated with FR-D plus vehicle or wt-Gal-1, shows the localization of PlexinA4 in the neurite process (βIII-Tub^{+}). Magnification of white frame in each image, points the structural localization of PlexinA4 clusters shown with a colocalization mask plug-in from Fiji image software. Additionally, a double staining plus FR-D shows the localization of PlexinA4 regarding FR-D. White arrowheads indicate the localization of PlexinA4 clusters alone in vehicle treated and localizing together with FR-D in wt-Gal-1-treated cells. Scale bars, 10 μm, 5 μm and 3 μm, respectively. Right bar graph shows a quantitative analysis of PlexinA4 cluster localization. Values represent the mean ± S.D. of three independent experiments ($n = 7$ cells analyzed per condition). $^{***}P < 0.05$ using one-way ANOVA followed by Bonferroni's Multiple Comparison Test.

containing cDNA particles was discarded and replaced by Neurobasal medium supplemented with B27, Glutamax, sodium pyruvate and a mix of penicillin-streptomycin (Wilson et al., 2015). Experiments were performed 36 h and 18 h after cDNA Hyper and cDNA Lifeact transfection (days *in vitro* 1,5). Efficiency of transfection was ~10%. All reagents used were purchased from Life technologies (CA, USA).

2.3. H_2O_2 detection using the HyPer biosensor in live cultured pyramidal neurons

After 24 h of HyPer expression, coverslips containing neurons were mounted in a cell thermostatic chamber (37 °C) to allow live-images acquisition using a confocal video-microscopy. During this process,

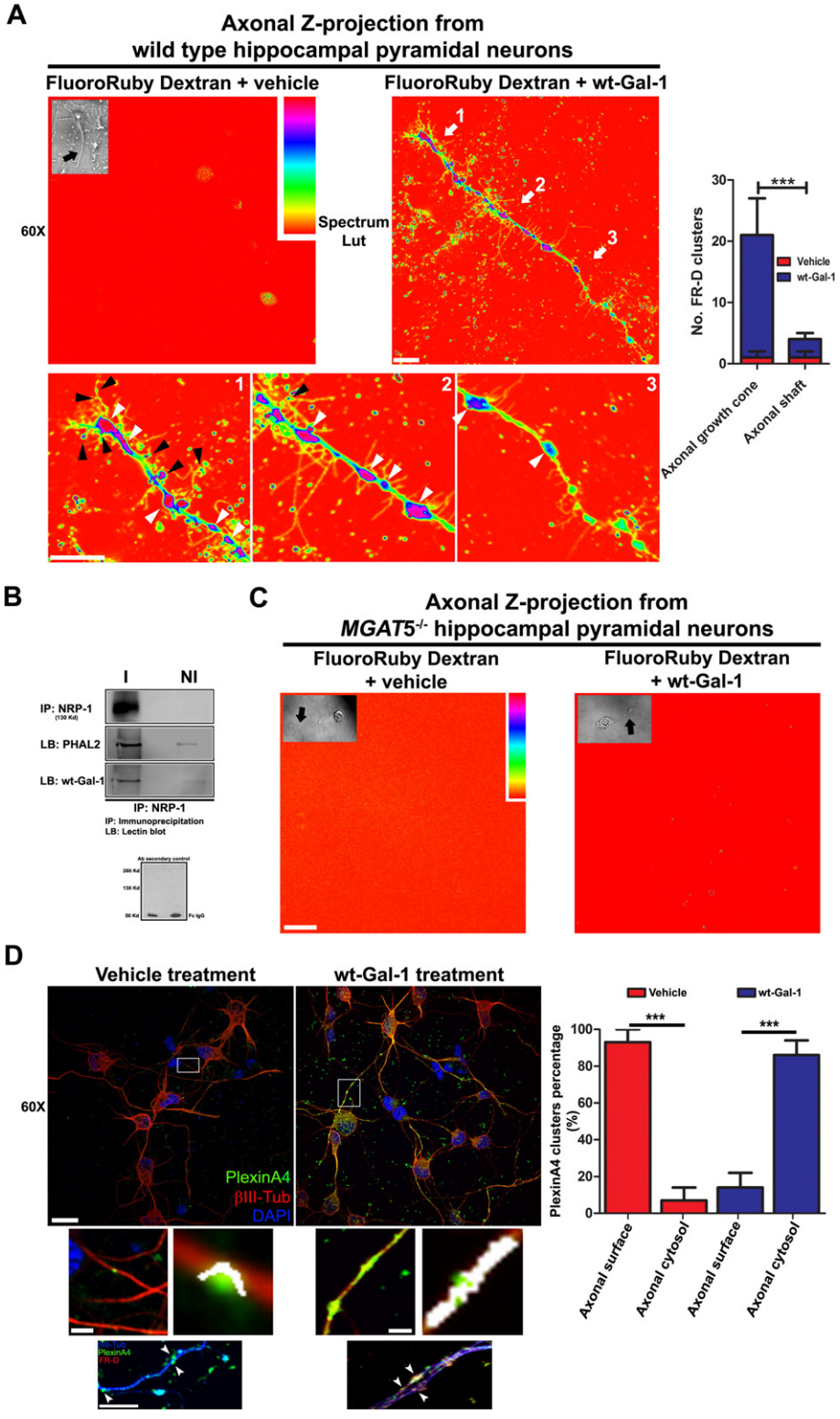

neurons were maintained in Hank's Balanced Salt Solution (HBSS) supplemented with HEPES buffer. To measure H_2O_2 content in live neurons, transfected cells were excited at 488 and 405 nm every 30 s for the indicated time in each figure. The emission was collected at 505–530 nm in both cases. Fluorescence emission from excitation at 488 nm was divided by fluorescence emission at 405 nm excitation (488:405), as a measure of H_2O_2 content (Belousov et al., 2006). To generate a H_2O_2 map, the ratio 488:405 was divided by the binary mask of the transfected cell (Wilson et al., 2015). Images were acquired using a Zeiss LSM 710 confocal microscopy using a 63× Plan-Apochromat Oil/1.4 N.A objective, airy unit = 1 airy-disk and linear scanning mode.

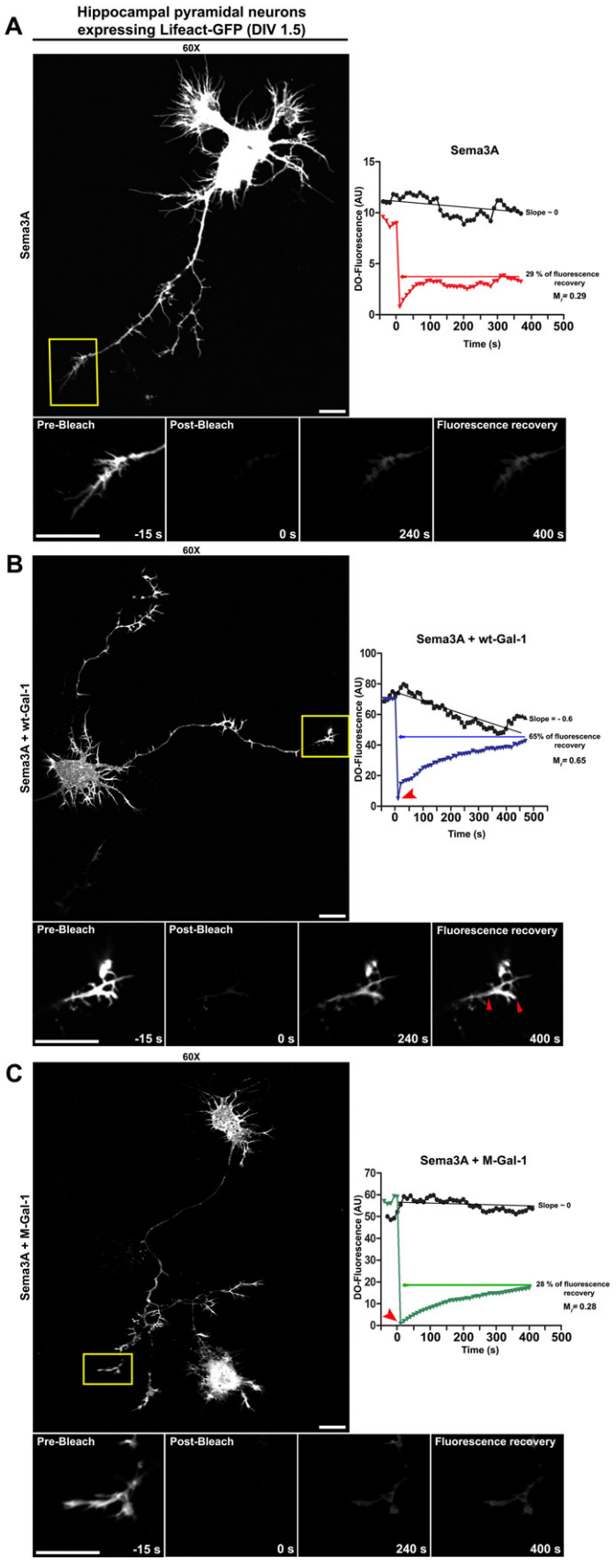

2.4. Gal-1^{Alexa488} internalization assay in live cultured pyramidal neurons

Wild-type recombinant Gal-1 occurring in a dimerization equilibrium (concentration > 7 μM) was tagged with Alexa Fluor® 488 Microscale Protein Labeling kit (Molecular Probes) following the manufacturer's instructions. The degree of labeling (DOL) of Alexa Fluor® 488 dye–labeled protein conjugate was determined obtaining the protein concentration by absorbance at 280 nm (A280) and at 494 nm (A494) using a NanoDrop 2000 (Thermo Scientific). Then, pyramidal neurons treated with wt-Gal-1^{Alexa488} (280 μg/ml) were mounted in a cell thermostatic chamber where the internalization process was tracked through 4D confocal microscopy (XYZT). The acquisition of Z-series optical slices (airy unit = 1 airy disk in accordance with Nyquist theory, optimum overlapping to minimize photobleaching) (Quinta et al., 2014b) was carried out every 30 s during 15 min, using a Zeiss LSM 710 confocal microscope, with a 60× Plan-Apochromat Oil/1.4 N.A objective. Excitation was applied at 488 nm and the signal emission was collected at 505–530 nm. Neuronal surface clusters were quantified using Measurement Point plug-in from Imaris 3D software 6.3.1 (Bitplane Sci Software, Zürich, Switzerland). Each surface cluster in XYZ was localized and projected for each time analyzed generating individual images. The surface clusters were quantified in each generated image. Particle tracking was performed using a Manual Tracking plug-in from Fiji software (v.1.45) (NIH; Bethesda, MA, USA). The images of each independent experiment were measured four times and averaged for each condition.

To evaluate whether this process belongs to ligand-mediated endocytosis, pyramidal neurons were treated for 15 min with 2 mg/ml FluoroRuby-conjugated Dextran from Molecular Probes (Eugene, OR, USA) plus wt-Gal-1 (280 μg/ml) or vehicle. Then, neurons were mounted in a cell thermostatic chamber where the internalization process was tracked through 4D confocal microscopy (XYZT) as explained above.

2.5. Measurement of actin cytoskeleton dynamics by fluorescence recovery after photobleaching

After 18-h Lifeact-GFP biosensor transfection, neurons were mounted in a cell thermostatic chamber on a confocal microscope setup. The region of interest (ROI) was defined (growth cone axon) and 5–10 images were acquired (pre-bleach) every 30 s with a rest time of 10 s. Then, the bleach was performed using Tornado-ROI function (allows rapid bleaching and laser light stimulation of desired fields) with a pixel time of 400 μs/pixel and 90% laser beam intensity. Post-bleach, the complete loss of fluorescence signal was verified. ROI images were then collected every 30 s during 9 min using an OlympusFluoview 1000 Confocal Microscope (Olympus Headquarters Corporate, Philadelphia, PA, USA) with 60× Plan-Apochromat Oil/1.42 N.A objective. The

Fig. 5. Reactivation of actin cytoskeleton dynamics at the axonal growth cone post-Sema3A treatment. (A), (B) and (C) Representative image of a neuron expressing Lifeact-GFP treated with: 300 μg/ml of Sema3A; 300 μg/ml of Sema3A plus 280 μg/ml of wt-Gal-1; 300 μg/ml of Sema3A plus 280 μg/ml of M-Gal-1. Yellow frame defines the bleach area of the axon growth cone. The magnifications are shown below each image. Scale bar, 10 μm. Right graphs of each images show a quantitative analysis of fluorescence recovery post-bleaching. Black lines correspond to fluorophore lifetime control. Red arrowhead in graphs (B) and (C) point the wt-Gal-1 and M-Gal-1 addition respectively. Value of mobile fraction (Mf) in each condition was measured in three independent experiments showing similar results.

mobile fraction and the percentage of fluorescence recovery were determined according to Ishikawa-Ankerhold (Ishikawa-Ankerhold et al., 2012).

$$Mf = \frac{I\infty - Io}{Ii - Io}$$

Mf = Mobile fraction; *Ii = Initial (pre-bleach) fluorescence intensity*; *I∞ = Maximal plateau value*; *Io = Low value*

$$I/2 = \frac{I\infty - Io}{2}$$

I/2 = Time for the exchange of half the mobile fraction between bleached and unbleached areas.

To rule out the possibility that changes in the fluorescence post-bleach could be associated with different levels of Lifeact-GFP expression, signal acquisition of background and measurement of fluorescence lifetime (in the non-bleached area) were analyzed in each image simultaneously to gain independence of the level of expression in each neuron. Also, to ensure that the expression level of Lifeact-GFP did not affect actin cytoskeleton dynamics, over-expression period did not exceed 18 h, as previously described (Wilson et al., 2015). Finally, a linear scanning mode plus digital zoom ×2 was used to ensure homogeneous excitation of samples, thus allowing quantitative fluorescence acquisition. The analysis was performed using integrated density plug-in from Fiji software (v.1.45) (NIH; Bethesda, MA, USA) normalized by area.

2.6. Real-time filopodial dynamics

After 18 h of Lifeact-GFP biosensor transfection, neurons were mounted in a cell thermostatized chamber on a confocal microscope setup. Time-lapse images were taken every 15 s for 15 min to visualize filopodial dynamics using an Olympus Fluoview 1000 Confocal Microscope (Olympus Headquarters Corporate, Philadelphia, PA, USA) with a 60× Plan-Apochromat Oil/1.42 N.A objective. Later, length of filopodia and movementof F-actin were measured using Measurement and Manual tracking plug-in from Fiji software (v.1.45) (NIH; Bethesda, MA, USA), respectively. Protrusions shorter than 2 μm and longer than 15 μm were not considered for analysis.

2.7. In vivo surgical procedures

Male C57BL/6 *Lgals1*$^{-/-}$ mice (kindly provided by F. Poirier, Jacques Monod Institut,

Paris, France) were used between 8 and 10 weeks of age (weight: 23–28 g). Animal care and treatment were carried out according to the guidelines of the Experimental Animal Care Committee of the School of Pharmacy and Biochemistry at the University of Buenos Aires, Argentina. Mice were anesthetized with ketamine (65 mg per kg body weight) and xylazine (15 mg per kg body weight) in a 600 ml solution to allow the anesthetic effect while still preventing a possible dehydration process (Quinta et al., 2014b). The SCI model was conducted at the Th9–Th10 lamina level as previously described (Bregman, 1987b, a; Quinta et al., 2014b). In brief, after laminectomy, the dura was opened and a complete transection of spinal cord was performed using a surgical blade. The severed ends were examined to check a complete transection. Then, 10 μl of wt-Gal-1 (1 μg/μl) was applied using microcapillary calibrated pipettes perpendicularly to the epicenter of the lesion site and in a 45° angle in both cranial and caudal orientation, as previously described (Quinta et al., 2014b). Control mice received the same volume of PBS. After treatment, the muscles and skin surrounding the lesion site were closed in layers. All the process was performed under a dissecting microscope. In the chronic SCI model, the wt-Gal-1 treatment was applied at the epicenter of the lesion site 2 months after injury. Anterograde labeling of CST axons was performed using FluoroRuby tracer (20%) from Molecular Probes (Eugene, OR, USA), eight days post wt-Gal-1 treatments (Chen et al., 2007; Quinta et al., 2015). The FR-D tracer was injected into the motor cortex at four different sites, 1 μl per site (AP coordinates from bregma in mm: AP 1.5/1.5,1.0/1.5, 0.5/1.5, 0.5/1.5 all at a depth of 0.5 mm into cortex) as previously described (Liu et al., 2010). The process was carried out under a Leica S4E stereo microscope (Wetzlar, Germany). After both surgeries, the mice were kept warm in an incubator at 28 °C for 2 h. Food was provided on the cage floor and water bottles were placed within reach.

2.8. Immunohistochemistry

Animals were transcardiacally perfused with PBS/heparin (0.05% *v*/*v*) followed by 4% paraformaldehyde in PBS. Spinal cords were removed and post-fixed overnight (ON) in the same fixative solution, then treated with a sucrose gradient (15 to 30%) and washed with PBS. Tissue was then frozen to obtain 30-μm cryostat longitudinal (cranial to caudal and dorso to ventral) sections using a Leica CM 1850 cryotome (Pasquini et al., 2011). To perform the analysis, 11 serial sections of spinal cord were collected from each specimen (vehicle control *vs* wt-Gal-1) and, using a free floating technique, the immunohistochemistry was carried out for a particular antigen or antigen pair as previously described by (Katherine Zukor,1 Stephane Belin,1 Chen Wang,1 Nadia Keelan,1,2 Xuhua Wang,1 and Zhigang He1). Slices were first incubated with high ionic force blocking buffer (HIFBB) for 50 min and later treated with 0.1% Triton X-100 in PBS for 14 min for permeabilization. Solutions for all primary antibodies were prepared in HIFBB and incubated for 3 h at room temperature, while secondary antibodies were incubated ON at 4 °C. Nuclear labeling was performed with 4′,6-diamidino-2-phenylindole (DAPI) for 1 h at room temperature. Controls to determine non-specific binding were performed using sections treated only with secondary antibodies using different IgG isotypes. All analyses were performed by an observer blinded to experimental conditions.

2.9. Behavior experiments

To assess the effects of wt-Gal-1 treatment on coordinated motor skill recovery, we used two behavioural tests:

2.9.1. Rotarod test

Treated, control and sham *Lgals1*$^{-/-}$ mice were placed in the rotarod as previously described (Bergeron et al., 2014). The speed used was 10 rpm. Mice were tested during 1 min with a latency period of 10 s. Three trials with 2 min of resting time were carried out per session on three consecutive days (13, 14 and 15) for each animal condition and the values were averaged. Trial end was considered when mice fell off the rod or when mice reached 1 min. Before starting the evaluation, animals were acclimatized in the sound-attenuated experiment room.

2.9.2. 90° grid walking test

A straight bridge-shaped metal grid was placed at 90° from the floor, as previously described (Quinta et al., 2014b) with modifications. Mice were placed at the base and the number of foot fall errors where the hindlimb failed to grasp a bar was recorded (0–10 scale) per climb. Three repetitions with 2 min of resting time were done for each animal condition in each day and the values were averaged.

Analysis for both tests was developed later by two experimenters who were blind to the experimental design.

2.10. Statistical analysis

Graph-Pad Prism software Version 5.0 (Graph-Pad software, Inc., La Jolla, CA, USA) was used for data analysis. Results are the mean of at least three independent experiments (N = 3) presented as mean ± SD. Comparisons were performed using unpaired one-tailed Student's *t*-test or one-way analysis of variance (ANOVA) followed by Tukey's

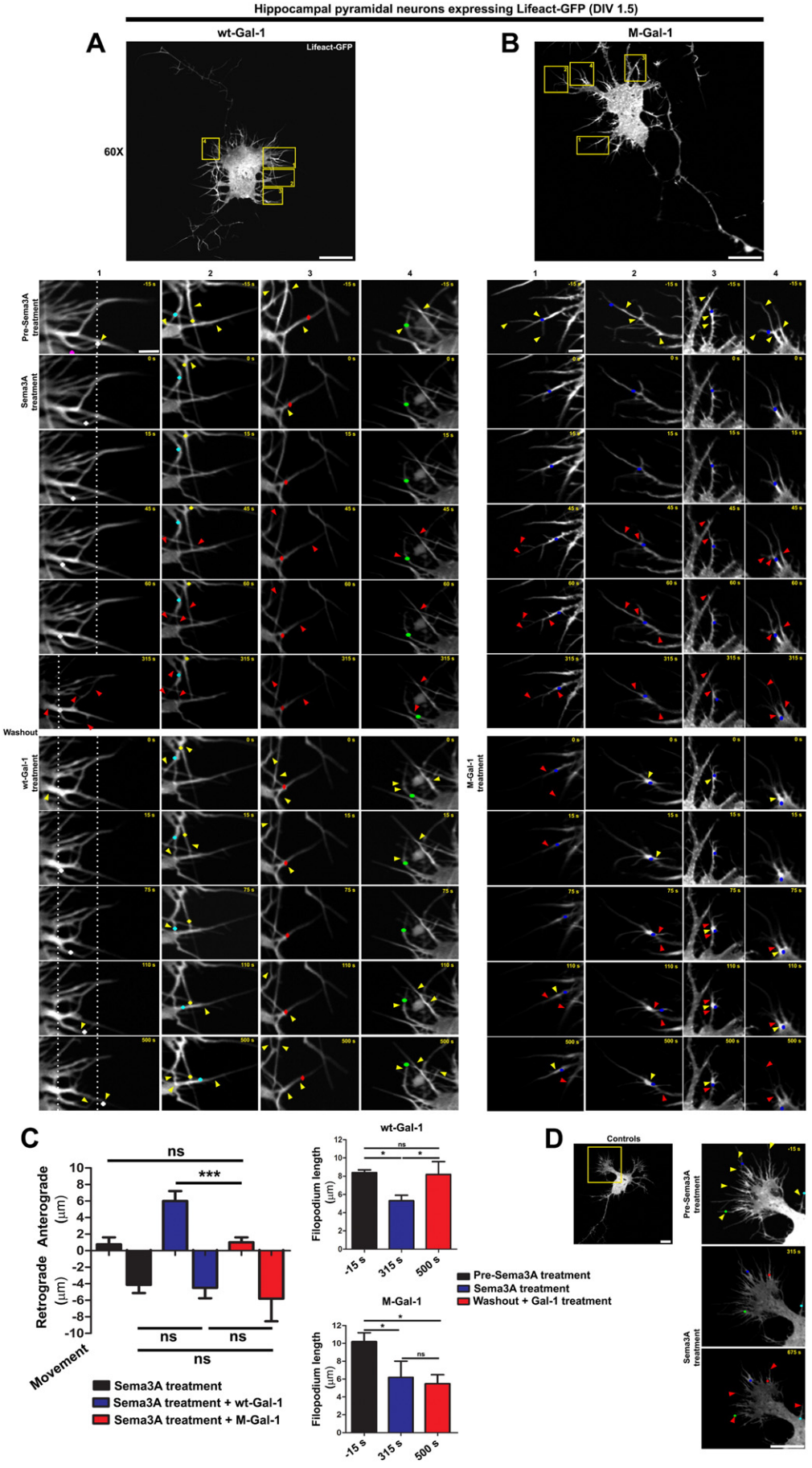
Hippocampal pyramidal neurons expressing Lifeact-GFP (DIV 1.5)
A
wt-Gal-1
Lifeact-GFP
60X
B
M-Gal-1
1
2
3
4
Pre-Sema3A treatment
Sema3A treatment
Washout
wt-Gal-1 treatment
M-Gal-1 treatment
C
Retrograde (µm)
Anterograde (µm)
Movement
ns
***
Sema3A treatment
Sema3A treatment + wt-Gal-1
Sema3A treatment + M-Gal-1
wt-Gal-1
M-Gal-1
Filopodium length (µm)
-15 s
315 s
500 s
Pre-Sema3A treatment
Sema3A treatment
Washout + Gal-1 treatment
D
Controls
Pre-Sema3A treatment
Sema3A treatment

post hoc tests or Bonferroni's Multiple Comparison Test, where appropriate.

3. Results

3.1. Treatment with wild-type recombinant Gal-1 decreases neuronal H_2O_2 production triggered by Sema3A

To determine whether Gal-1 may counteract H_2O_2 levels triggered by Sema3A, we examined, in real time, whether H_2O_2 levels in pyramidal neurons were modified by the pre-addition of: wt-Gal-1 (wild-type recombinant Gal-1 form occurring in a dimer equilibrium, 280 μg/ml) (Quinta et al., 2014b); M-Gal-1 (a stable monomeric mutant, 280 μg/ml) and Gal-1-N46D (mutant lacking carbohydrate-binding activity, 280 μg/ml). Cultured pyramidal neurons isolated from embryonic hippocampus transfected with the HyPer biosensor were treated in situ with a Sema3A-conditioned medium (300 μg/ml, 20 nM) to promote complete growth cone collapse (>85%) (Antipenko et al., 2003; Mire et al., 2008). H_2O_2 production was measured in the same neuron every 30 s during 15 min. Control of basal intraneuronal H_2O_2 production was performed only with DMEM supplemented with 2.5% FBS (vehicle of Sema3A). Whereas exposure to Sema3A promoted a rapid increase in intraneuronal H_2O_2 levels together with varicosity (axonal sprout site) collapse (Fig. 1A), pre-treatment with wt-Gal-1 before Sema3A addition induced a significant decrease in intraneuronal H_2O_2 levels. However, pre-treatment with M-Gal-1 only induced slight inhibition, suggesting a major role for Gal-1, in its dimeric form, in regulating H_2O_2. In contrast, treatment with Gal-1-N46D, not only failed to prevent Sema3A effects, but also increased them to higher levels than those observed with Sema3A alone (Fig. 1A and 1B), suggesting that protein-carbohydrate interactions may play a major inhibitory role in tuning NRP-1/Plexin4A signaling. Based on these findings, we next conducted a sequential time lapse experiment where Sema3A was first added and the increment in H_2O_2 levels was measured during 11 min. Addition of wt-Gal-1 after this time period produced a significant decrease in high pre-existing H_2O_2 levels, while prevented a further increase induced by second exposure to Sema3A (Fig. 2A and 2B). Finally, pyramidal neurons expressing HyPer biosensor were incubated with Sema3A; wt-Gal-1; M-Gal-1; wt-Gal-1 plus Sema3A and M-Gal-1 plus Sema3A, for 24 h. We found a significant decrease in H_2O_2 level regarding Sema3A control in neurons treated with wt-Gal-1 or in competition with Sema3A, showing comparable values to those observed under basal conditions (control). Accordingly, only those neurons showed axonal growth. In contrast, treatment with M-Gal-1, which was unable to bind to the NRP-1/PlexinA4 receptor in its monomeric conformation (Quinta et al., 2014a, 2014b), did not prevent H_2O_2 production by Sema3A in pyramidal neurons (Fig. 2C and 2D).

3.2. Wild-type recombinant Gal-1 binds to Neuropilin on the neuronal surface and is rapidly internalized

We recently demonstrated that only wt-Gal-1, when presented in its dimeric equilibrium, binds to the NRP-1/PlexinA4 receptor on the neuronal surface promoting axonal regeneration and preventing Sema3A binding (Quinta et al., 2014b). Moreover, it is well known that ligand-mediated endocytosis is actively stimulated by Sema3A, when it binds to NRP-1/PlexinA4 receptor, triggering a retrograde vesicular axonal transport (Goshima et al., 1997; Fournier et al., 2000). However, the signaling events associated with Gal-1 binding remain uncertain. Our results using 4D confocal microscopy (XYZT) show that wt-Gal-$1^{Alexa488}$ added to pyramidal neurons is internalized in 15 min (Fig. 3A). We found a significant drop in the number of wt-Gal-$1^{Alexa488}$ clusters on the neuronal surface, with ~63% of the fluorescent protein being internalized (309 ± 21 clusters at time 0 min and 117 ± 30 clusters after 15 min at neuronal surface) (Fig. 3B). Moreover, during this period, no significant changes were observed in the lifetime Alexa Fluor 488 fluorescence (Fig. 3B inset) and no traces of wt-Gal-$1^{Alexa488}$ were detected in the acquisition medium during the internalization process. Additionally, a representative movement of wt-Gal-1 clusters was tracked from the neuronal surface (Fig. 3C, 0 min) toward internal compartments of the axon (Fig. 3C, 14 min), revealing a retrograde trajectory of 10 ± 0.8 μm (Fig. 3C, right panel).

3.3. Gal-1, in its dimeric form, promotes ligand-mediated endocytosis of the PlexinA4 receptor via N-glycan recognition

Endocytosis triggered by Sema3A promotes internalization of PlexinA4 with concomitant growth cone collapse (Fournier et al., 2000). In the case of pyramidal neurons, even though wt-Gal-1 prevents growth cone collapse and stimulates axonal regeneration, it is uncertain whether this treatment could also promote ligand-mediated internalization of PlexinA4. Interestingly, axonal growth cone of pyramidal neurons exposed to wt-Gal-1 in the presence of FluoroRuby-conjugated dextran (FR-D) evidenced a significant internalization of dextran compared to vehicle control. Accumulation of FR-D was evident not only inside the growth cone but also in the proximal axonal shaft within only 20 min (Fig. 4A), demonstrating that the uptake of FR-D occurred preferentially in the axonal growth cone with a retrograde movement of FR-D to the axonal shaft (Fig. 4A (inset 1; 2; 3), right bar graph). Notably, these effects were in line with those observed upon Sema3A treatment as previously described (Fournier et al., 2000). Ligand-mediated endocytosis was triggered only when dimeric Gal-1 bound to the NRP-1 complex through interaction with β1-6-*N*-acetylglucosamine (β1-6GlcNAc)-branched complex N-glycans, as shown by binding of the *Phaseolus vulgaris* leucoagglutinin (PHA-L) lectin (Fig. 4B). However, when FR-D internalization was studied in pyramidal neurons from mice lacking the β1,6-*N*-acetylglucosaminyltransferase 5 (MGAT5), an enzyme responsible of generating β1-6GlcNAc-branched complex N-glycans, which are central intermediates for LacNAc extension (preferred ligands for galectins) (Croci et al., 2014), treatment with wt-Gal-1 could not trigger ligand-mediated endocytosis, suggesting dependence of complex N-glycan recognition to trigger the endocytic process (Fig. 4C). Finally, wild type pyramidal neurons treated with wt-Gal-1, which internalized FR-D (Fig. 4A) also internalized PlexinA4 from the axonal surface to the cytosol as compared to vehicle treatment (PBS) ($P < 0.05$, Fig. 4D). Insets in Fig. 4D show a representative PlexinA4 cluster (at high magnification) surrounding the axonal shaft (visualized with a thin colocalization mask) in neurons treated with vehicle. Notably, there was a complete absence of FR-D uptake. In contrast, in neurons treated with wt-Gal-1, a thick colocalization mask was visualized inside the axon. Besides, the colocalization between FR-D and PlexinA4 inside the axon supports internalization. Of note, immunolabeling was performed under permeabilization conditions to rule out the possibility of false negative results regarding the presence of PlexinA4 clusters in the axonal cytosol following vehicle treatment.

Fig. 6. Filopodial F-actin dynamics post-Sema3A treatment. Representative time-lapse images of neurons expressing Lifeact-GFP treated with 300 μg/ml of Sema3A followed by washout and addition of: (A) 280 μg/ml of wt-Gal-1 or (B) M-Gal-1. Yellow frame in each condition point different fillopodium around the neuron. Magnification of each frame are shown below. Color dots point in each panel the localization of last segment of F-actin tracked. Yellow arrowhead shows the presence and red arrowhead shows the absence of Lifeact in the fillopodium. Scale bar, 20 μm and 2.5 μm, respectively. (C) Quantification of the movement and length of filopodia from (a) and (b) insets. Values represent the mean ± S.D. of three independent experiments. $^{***}P < 0.001$, $^{*}P < 0.05$ and NS = not significant using one-way ANOVA followed by Tukey's tests. (D) Control of F-actin fluorescence intensity decrease and filopodial shortening, after Sema3A treatment. The inset shows the growth cone, where the red arrowhead points the filopodial shortening after Sema3A treatment. Scale bar: 10 μm.

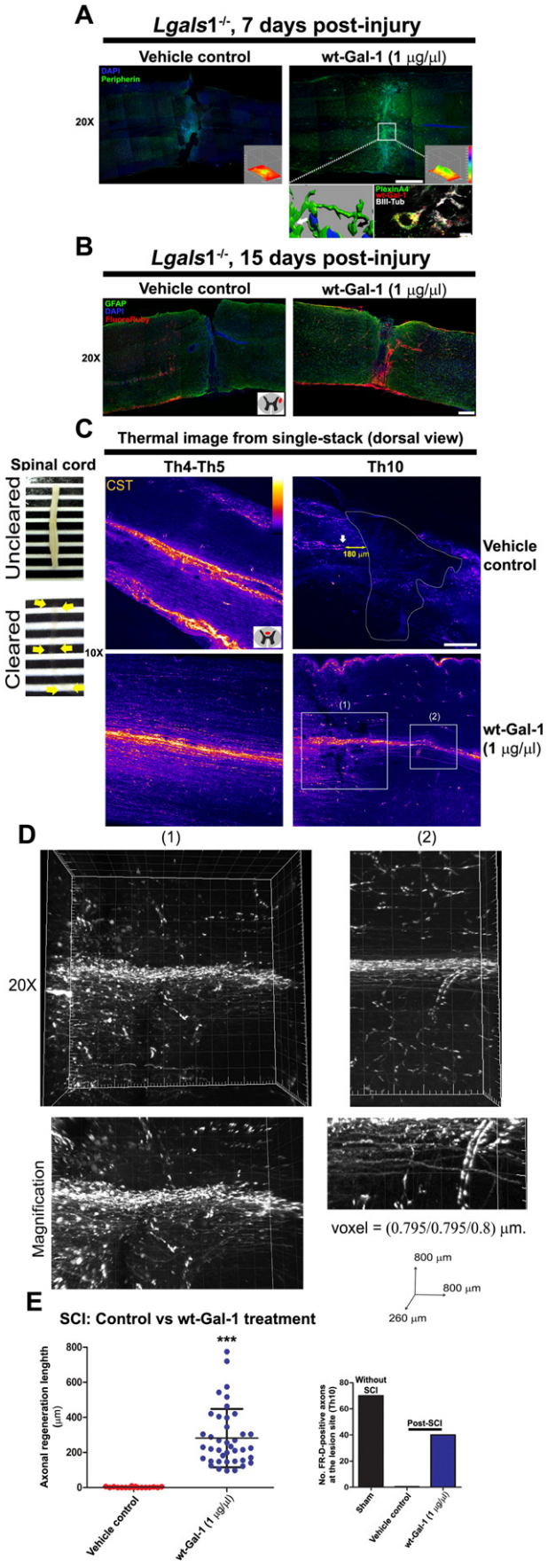

3.4. Wild-type recombinant Gal-1 reactivates actin cytoskeleton dynamics at the axonal growth cone following the collapse triggered by Sema3A

To determine whether the decrease in H_2O_2 levels induced by Gal-1 treatment favors reactivation of actin cytoskeleton dynamics, a Fluorescence Recovery after Photobleaching (FRAP) technique was applied in the growth cone of pyramidal neurons$^{Lifeact\text{-}GFP}$ (transfected with genetically encoded probe Lifeact, which allows real time visualization of actin polymerization (Riedl et al., 2008)). The neurons were treated with Sema3A and pre-bleached images were taken during 2.5 min. Then, photobleaching was applied in the growth cone (ROI) and, post-bleaching, the fluorescence recovery was measured in real time, reaching only 29% of total fluorescence (control) with a mobile fraction of 0.29 (Fig. 5A). Neurons to which wt-Gal-1 post-Sema3A treatment was added reached post-bleach, a fluorescence recovery of 65% with a mobile fraction of 0.65 (Fig. 5B). In contrast, neurons exposed to M-Gal-1 post-Sema3A treatment reached similar levels of fluorescence recovery as those observed with Sema3A control with comparable mobile fraction (0.29 *vs* 0.28, respectively) (Fig. 5C). Fluorescence lifetime in each experiment during the time-lapse, was in turn measured. The slope of fluorescence lifetime was ~0 in Sema3A control and M-Gal-1 treatment. In contrast, the fluorescence fluctuation was ~− 0.6 upon wt-Gal-1 treatment, suggesting that fluorescence recovery could be even higher.

3.5. Wild-type Gal-1 reactivates movement of filopodial F-actin at the neuronal surface as well as filopodial re-growth post-Sema3A treatment

Filopodial dynamics was evaluated by tracking the movement of F-actin and measuring filopodia length in neurons$^{Lifeact\text{-}GFP}$. Before treatment, neurons showed strong fluorescence intensity of F-actin with large filopodia. Addition of Sema3A promoted in every tested condition (control, pre-wt-Gal-1 and pre-M-Gal-1) a sharp decrease in F-actin fluorescence intensity plus a retrograde movement and filopodial shortening in the time lapse of the experiment (Fig. 6A and 6B) similarly as previously reported (Fournier et al., 2000). However, post-washout, addition of wt-Gal-1 promoted a recovery in F-actin fluorescence intensity together with a significant recovery in anterograde F-actin movement, overcoming the distance reached in the retrograde motion triggered by Sema3A. Moreover, wt-Gal-1 treatment also promoted a significant recovery in filopodial elongation, which reached the same length observed in neurons before Sema3A treatment (Fig. 6A (post-washout) and C). Interestingly, this length was similar to that observed in normal pyramidal neurons (DIV 1.5) as described (Wilson et al., 2015). In contrast, addition of M-Gal-1 could not restore F-actin fluorescence intensity, which showed punctuate aggregates, and failed to promote anterograde movement (no significant differences regarding Sema3A treatment). Furthermore, M-Gal-1 could not restore the length of filopodium observed in neurons before Sema3A treatment and rendered the same filopodial features observed upon Sema3A treatment (Fig. 6B (post-washout) and C). Fig. 6D shows a control of growth cone collapse after Sema3A treatment.

Fig. 7. Re-growth of corticospinal tract in *Lgals1*$^{-/-}$ mice with SCI treated with wild-type recombinant Gal-1. (A) Representative double staining with Peripherin and DAPI. Inset shows the Peripherin expression using 3D surface plot plug-in from Fiji program. White frame in right image shows the regenerated neurons at the lesion site. Left inset shows a render of regenerated neuron. White arrow shows the soma and black arrow shows the non-collapsed growth cone. Right inset shows a triple staining with PlexinA4, wt-Gal-1 and βIII-Tub. Scale bar: 250 μm and 10 μm, respectively. (B) Immunohistochemical analysis of dlCST labeling post-SCI. Scale bar, 250 μm. (C) Images of whole dCST acquired using one-photon microscopy by clearing technique. Dotted white line delimits the lesion area in vehicle control and white arrow point the distance of "dye back" from the lesion site. Scale bar, 250 μm. (D) 3D-magnification of regenerated CST (wt-Gal-1 treatment) pointed in the white frame from (C). (E) Graph shows a quantitative analysis of the number and length of axonal regeneration. Inset graph correspond to a quantification of FR-D-positive axons at Th10. Values represent the mean ± S.D. of three independent experiments (n = 4 mice per group). ***$P < 0.0001$ using unpaired *t*-test.

3.6. Treatment with wild-type Gal-1 promotes re-growth of corticospinal tract and coordinated locomotor recovery post complete transection of spinal cord in *Lgals1*$^{-/-}$ mice

Recently, we have been demonstrated that Gal-1 treatment promotes axonal regeneration at the lesion site in an SCI mice model (Quinta et al., 2014b). However, there are no reports on its effects on the injured corticospinal tract (CST), the major neural pathway for the control of voluntary movement and the only direct pathway from the motor cortex to the spinal cord (Liu et al., 2008; Quinta et al., 2015). Interestingly, whereas a sharp increase in the expression of the chemorepulsive Sema3A protein is evident in post-SCI (Kaneko et al., 2006), wt-Gal-1 promoted a decrease in H_2O_2 content and reactivation of F-actin dynamics at the axonal growth cone. Although endogenous Gal-1 did not promote axonal re-growth (Quinta et al., 2014b, a), we carried out *in vivo* experiments using *Lgals1*$^{-/-}$ mice to evaluate the physiological relevance of Gal-1 treatment on axonal growth. Treatment with wt-Gal-1 (1 μg/μl) promoted axonal re-growth at the lesion site compared with vehicle control (PBS) as visualized by immunohistochemical analysis using the specific axonal regenerating marker Peripherin (Fig. 7A). Moreover, using the Imaris 3D program 6.3.1, we found a surface render (Quinta et al., 2010; Quinta and Galigniana, 2012) of a regenerated axon with its non-collapsed axon growth cone at the lesion site, along with the internalization of PlexinA4 and wt-Gal-1; these proteins were detected at the same focal plane (Fig. 7A; insets). Furthermore, assessment of re-growth of dorso-lateral CST (dlCST) developed by classical histological sectioning (Brambilla et al., 2009; Zukor et al., 2013) showed that treatment of *Lgals1*$^{-/-}$ mice with wt-Gal-1 induced re-growth of dlCST, which was tagged with FR-D (Fig. 7B). Moreover, using the three-dimensional CST reconstruction by a clearing technique (Quinta et al., 2015), we measured the number and length of each regenerated axonal tract post-dorso CST (dCST) disruption. Our results show that the whole cleared spinal cord from *Lgals1*$^{-/-}$ mice treated with wt-Gal-1 presented a sharp re-growth of damaged axons, which crossed the lesion site as compared to the effects observed following treatment with vehicle control, where axons exhibited a truncated trajectory showing a "die back" starting at 180 ± 5 μm from the lesion site (Fig. 7C). The surpass images show the shape of regenerated cortical axons at the lesion site as well as downstream areas (Fig. 7D, inset 1–2 of Fig. 7C and movies S1 and S2). Finally, we found a significant difference in the number of regenerated axons and their length downstream of the lesion site in each experimental condition (vehicle control *vs* wt-Gal-1 treatment) ($P < 0.0001$, Fig. 7E). In line with these findings, *Lgals1*$^{-/-}$ mice treated with wt-Gal-1 evidenced a significant increase in axonal tract re-growth in the junction between white and gray matter at the lesion site, as compared to the complete absence of axonal tracts in vehicle control-treated mice ($P < 0.0001$, Fig. 8A). Moreover, this treatment promoted the neo-formation of pre-synaptic cluster in the regenerated axons, not only in the axon terminal (Fig. 8A, inset in Y/Z and X/Z), but also in the shaft. Interestingly, only in mice treated with wt-Gal-1, downstream areas at the lesion site showed normal distribution of Synapsin-1, a pre-synaptic marker, over the motoneurons surface (Fig. 8A, right inset and bar graph below). These results demonstrate that the re-growth of axonal tracts prevents trans-synaptic degeneration. In addition, we quantified Synapsin-1 cluster neo-formation at the whole lesion site by confocal Z-scanning followed by signal conversion into a 3D-render spot (Fig. 8B). On the basis of these findings, we evaluated whether the pre-synaptic component of regenerated axons correlated with post-synaptic density, labeled with PSD-95 (post synaptic density of 95 Kd), at the lesion site. A quantitative correlation analysis using Pearson's coefficient showed 30% colocalization between each Synapsin-1 and PSD-95 cluster in wt-Gal-1-treated *Lgals1*$^{-/-}$ mice (Fig. 8C). The rate of overlapping between pre- and post- synaptic markers correlated with that observed in the formation and remodeling of postsynaptic density as previously described (Marrs et al., 2001). To support the notion that axonal tracts re-growth, triggered by wt-Gal-1 treatment acquires functional properties, we also evaluated their myelination state. In a chronic spinal cord injury model, we observed that the whole cleared spinal cord from vehicle-treated *Lgals1*$^{-/-}$ mice exhibited a complete absence of axonal tracts in white matter, as well as Olig-2- (oligodendrocyte transcription factor encode by the Olig-2 gene)-positive cells. In contrast, upon wt-Gal-1 treatment, we found an increase in regenerated neurofilament-positive axons in white matter together with Olig-2-positive cells (Fig. 8D). Besides, the neurofilament-positive segments exhibited oligodendrocytes in their vicinity, sandwiched and spaced 35 ± 6 μm from each other (Fig. 8D, insets). Finally, we analyzed the behavior of *Lgals1*$^{-/-}$ mice subjected to SCI and further treated with wt-Gal-1 or with vehicle control. To assess mice voluntary coordinated locomotion (which depends on corticospinal tract integrity (Liu et al., 2008; Quinta et al., 2015)), we used the rotarod test and the 90° grid walking apparatus test. All mice suffered hindlimb paralysis immediately after transection. Whereas the vehicle-treated *Lgals1*$^{-/-}$ mice showed virtually no recovery in locomotor activities (average latency to fall in rotarod test was ~0 s, which did not significantly change throughout the test), *Lgals1*$^{-/-}$ mice treated with wt-Gal-1 showed a significant increase in locomotor coordination (average latency to fall ~56 s, improving the rate of fall throughout the test) reaching the values observed in sham mice (Fig. 8E). Furthermore, in the 90° grid walking apparatus test, vehicle-treated *Lgals1*$^{-/-}$ mice showed a high number of foot fall errors (9 ± 0.8), while *Lgals1*$^{-/-}$ mice treated with wt-Gal-1 showed a significant decrease in the number of foot fall errors (2 ± 0.7) ($P < 0.001$, Fig. 8F).

4. Discussion

We have previously identified Gal-1 as a novel regulatory protein capable of interrupting the Sema3A pathway *in vivo*, through binding to the NRP-1/PlexinA4 neuronal receptors and promoting full locomotor recovery post SCI (Quinta et al., 2014b). However, the mechanisms by which Gal-1 promotes, post NRP-1/PlexinA4 binding, axonal re-growth remained poorly understood. In a pathological situation such as SCI Sema3A is secreted by meningeal fibroblasts, being the first inhibitory molecule of axonal regeneration to reach the lesion site (Kaneko et al., 2006). Further, this molecule binds NRP1/PlexinA4 receptor on the neuronal surface, promoting a strong inhibition of CST re-growth by a dramatic growth cone collapse (Pasterkamp et al., 1999; Tamagnone et al., 1999; Kaneko et al., 2006). The signaling events underlying these pathological effects involve molecular and biochemical pathways including Sema3A-triggered F-actin disassembly and decreased ability to re-polymerize (Fan et al., 1993; Hung and Terman, 2011). F-actin depolymerization and collapse is promoted by oxidation of its methionine residues (M44 and M47) (Giridharan and Caplan, 2014). The ROS involved in the oxidation process is H_2O_2, whose production is promoted by MICAL activation, triggered in turn by PlexinA4-cytoplasmic domain Sema3A dependent-binding (Giridharan and Caplan, 2014). Nonetheless, it is important to highlight that physiological levels of ROS are indeed necessary for normal neuronal development and function (Wilson et al., 2015). Here, using quantitative confocal video microscopy, we demonstrate that only pre-exposure to wild-type recombinant Gal-1, which displays full dimerization capability and intact carbohydrate binding activity could prevent H_2O_2 production triggered by Sema3A. Remarkably, even though monomeric Gal-1 treatment could initially and partially prevent H_2O_2 production (Fig. 1), it failed to sustain this effect for longer periods (Fig. 2D). This short-lived effect was probably due to the high concentration of M-Gal-1 added, which forced to a minimum fraction of monomer to retain carbohydrate-binding capacity (Cho and Cummings, 1996; Barrionuevo et al., 2007) until the equilibrium was reached. Moreover, when Gal-1-N46D (mutant lacking carbohydrate-binding activity) was added, there was an increase in the H_2O_2 production, supporting the specificity of carbohydrate recognition activity. These data suggest that pre-treatment with wt-Gal-1 prevents

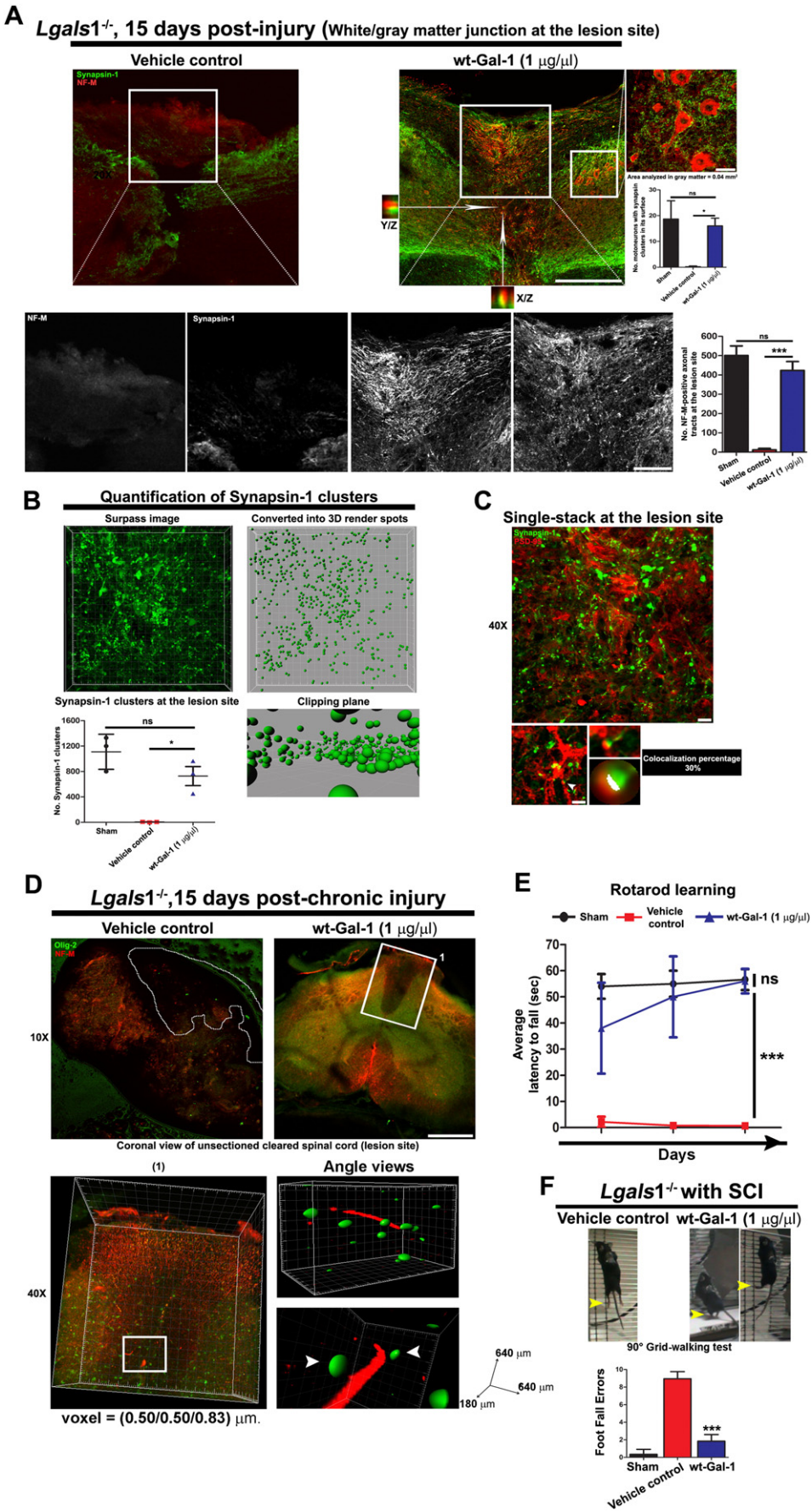
A
Lgals1-/-, 15 days post-injury (White/gray matter junction at the lesion site)
Vehicle control
wt-Gal-1 (1 μg/μl)
Synapsin-1
NF-M
Y/Z
X/Z
Area analyzed in gray matter = 0.04 mm²
No. motoneurons with synaptin cluster in its surface
ns
*
Sham
Vehicle control
wt-Gal-1 (1 μg/μl)
NF-M
Synapsin-1
No. NF-M-positive axonal tracts at the lesion site
ns
***
B
Quantification of Synapsin-1 clusters
Surpass image
Converted into 3D render spots
Synapsin-1 clusters at the lesion site
Clipping plane
No. Synapsin-1 clusters
C
Single-stack at the lesion site
Synapsin-1
PSD-95
40X
Colocalization percentage
30%
D
Lgals1-/-,15 days post-chronic injury
Vehicle control
wt-Gal-1 (1 μg/μl)
Olig-2
NF-M
10X
Coronal view of unsectioned cleared spinal cord (lesion site)
(1)
Angle views
40X
640 μm
640 μm
180 μm
voxel = (0.50/0.50/0.83) μm.
E
Rotarod learning
Sham
Vehicle control
wt-Gal-1 (1 μg/μl)
Average latency to fall (sec)
ns
***
Days
F
Lgals1-/- with SCI
Vehicle control
wt-Gal-1 (1 μg/μl)
90° Grid-walking test
Foot Fall Errors
***
Sham
Vehicle control
wt-Gal-1

Sema3A binding to NRP-1/PlexinA4 complex and thereby inhibits the intracellular production of H_2O_2. On the other hand, when pyramidal neurons were treated with Sema3A, the addition of wt-Gal-1 diminished the levels of H2O2 to basal. Besides, a second burst of Sema3A could not promote H_2O_2 production. This result suggests that Gal-1, mainly in its dimeric form, might have an intracellular specific function. This might be due to the fact that wt-Gal-1 is taken up by the NRP-1/PlexinA4 receptor at the neuronal surface (Quinta et al., 2014b) and then internalized. This process occurred in a short period of time, mimicking the internalization and retrograde movement of PlexinA4 triggered by Sema3A treatment (Goshima et al., 1997; Fournier et al., 2000). In addition, Sema3A-dependent binding to NRP-1/PlexinA4 receptor promotes endocytic events which cause the internalization of local membranes (Mann and Rougon, 2007).

The data presented in this study demonstrates that endocytosis of Gal-1 is a ligand-mediated process, as wt-Gal-1 treatment promotes neuronal internalization of FR-D, which only occurs in the presence of ligand-mediated endocytosis (Fournier et al., 2000). In addition, we show that endocytosis only takes place when wt-Gal-1 binds to NRP-1/PlexinA4 receptor through recognition of highly branched complex *N*-glycans. In this regard, pyramidal neurons from *Mgat5*$^{-/-}$ mice cannot promote FR-D internalization in presence of wt-Gal-1. Interestingly, most studies aimed at revealing MGAT5 function were carried out using pheochromocytoma cells transfected with glycosyltransferase *iRNA* (Yang et al., 2008), due to limitations in performing primary cultures of pyramidal neurons from *Mgat5*$^{-/-}$ mice. Given that pheochromocytome is not an appropriate neuronal model because these cell lines are not pyramidal neurons, we performed primary neuron cultures despite their low efficiency (one of the four postnatal mice was knockout). Additionally, we noticed that these cultures had some difficulties regarding their normal development mimicking the *in-vivo* events (Lee et al., 2007).

Finally, we found that PlexinA4 also was internalized from the axonal surface to the cytosol in the pyramidal neurons which showed FR-D uptake after wt-Gal-1 treatment (Fig. 4D). This result suggests that Gal-1, a Sema3A antagonizing protein (Quinta et al., 2014b), also promotes PlexinA4 internalization despite having opposite effects. Even though the internalization of PlexinA4 receptor complex occurs in the same manner that observed in presence of Sema3A, the endocytosis of wt-Gal-1 might block the cytoplasmic plexinA4 domain and, thereby, interrupt MICAL activation, preventing H_2O_2 production. Supporting this explanation, we show colocalization between wt-Gal-1 and PlexinA4 at intra-neuronal level only in a spinal cord tissue from wt-Gal-1-treated mice with SCI (Fig. 7A). Moreover, as our understanding of MICAL biochemistry is relatively new, we propose that Gal-1 might likely promote enzymatic activation, probably at the level of the glutathione system as well as other enzymes required for ROS homeostasis, in order to remove H_2O_2 (Limon-Pacheco and Gonsebatt, 2010).

When Sema3A binds to NRP-1/PlexinA4 receptor at the neuronal surface, post-internalization the cytoplasmic PlexinA4 domain causes actin cytoskeleton alterations in the growth cone (Negishi et al., 2005), which are due to increased H_2O_2 production. Here we demonstrate that Gal-1-NRP-1/PlexinA4 complex not only prevents H_2O_2 production but also triggers the reactivation of actin cytoskeleton dynamics. This process is clearly observed in the axonal growth cone post-collapse triggered by Sema3A, where new segments of F-actin are shaped. The recovery of fluorescence intensity in the axonal growth cone was ~65% in 400 s as compared to control (Fig. 5). In contrast, treatment with monomeric Gal-1 did not show significant differences regarding fluorescence recovery or F-actin neo-formation as compared to Sema3A treatment. Additionally, only treatment with wt-Gal-1 triggered a recovery in actin anterograde movement at the filopodium on the whole neuronal surface post-Sema3A addition. Besides, filopodia reached the same length as that observed in the pre-Sema3A treatment. These results strongly support the relationship between the decrease in H_2O_2 promoted by Gal-1-N-glycan interactions and the direct effect on actin cytoskeleton reactivation. Finally, we analyzed the effects of Gal-1 at >7 μM (a concentration that allows dimerization and leads to diminished H_2O_2 production and actin cytoskeleton reactivation) on damaged axons from pyramidal neurons in an *in vivo* SCI model. In addition, we evaluated the possible recovery of function in these regenerated axons, as well as post-injury behavior. We found re-growth of previously injured pyramidal axons (which form the CST dorsal and dorso-lateral) with regenerated axons on average almost reaching 300 μm distal to the lesion site within 15 days post-injury. Interestingly, the regenerated neurons which surrounded the lesion site exhibited internalization of PlexinA4, spread out in clusters in a similar fashion as that observed in *in vitro* experiments using wt-Gal-1. In contrast, vehicle-treated non-regenerated neurons showed sharp NRP-1 accumulation, as previously described (Quinta et al., 2014b).

Regarding the possible function of regenerated tracts, the localization of Synapsin-1 clusters in the axons at the lesion site, as well as the colocalization with PSD-95 confirmed the presence of neo-synaptic pathways. The movement and remodeling of these structures depend on actin-based dynamics to drive filopodial protrusion (Halpain, 2000; Matus, 2000). Besides, we detected myelinated oligodendrocytes surrounding the regenerated axons. Also, as the model used was a chronic SCI, addition of wt-Gal-1 promoted axonal re-growth after Sema3A secretion, which confirms that this treatment promotes reactivation of the actin cytoskeleton.

Concerning behavior assays, only mice treated with wt-Gal-1 showed recovery of locomotor coordination. This effect could be explained by the arrangement of intraspinal neural circuits between regenerated axons, most probably from interneurons at the lesion site, which produced signal relay and synaptic connections with the regenerated corticospinal tract as previously described (Bareyre et al., 2004; Kaneko et al., 2006). We also show the absence of trans-synaptic degeneration (Fig. 8A, right inset). In summary, the results presented here provide a mechanistic explanation for the inhibitory role of Gal-1 on Sema3A interactions with the NRP-1/PlexinA4 complex. Axonal tract re-growth correlated with the decrease in H_2O_2 content and concomitant actin cytoskeleton dynamics reactivation. This event occurred via

Fig. 8. Neo-formation of pre-synaptic cluster in regenerated axons and evaluation of coordinated locomotor recovery in *Lgals1*$^{-/-}$ mice with SCI treated with wild-type recombinant Gal-1. (A) Double staining with NF-M and Synapsin-1. Magnification of insets in each condition is shown below. Mice treated with wt-Gal-1 showed colocalization between NF-M and Synapsin-1 (X/Z and Y-Z). Motoneurons with normal synaptic contact are shown in downstream areas (highlighted in the right white frame). Bar graph below shows a quantification of motoneurons with Synapsin-1 cluster in its surface. Values represent the mean ± S.D. of area analyzed in each tissue slide of three independent experiments (n = 3 mice per group). $^{*}P < 0.05$ and NS = not significant using one-way ANOVA followed by Tukey's tests. Right bar graph shows the quantification of regenerated axonal tracts. Values represent the mean ± S.D. of three independent experiments (n = 3 mice per group). $^{***}P < 0.0001$ and NS = not significant using one-way ANOVA followed by Tukey's tests. Bar scale, 250 μm and 100 μm, respectively. (B) Representative 3D-images of Synapsin-1 clustering. Graph shows a quantification of neo-cluster at the lesion site. Values represent the mean ± S.D. of three independent experiments (n = 3 mice per group). $^{*}P < 0.05$ and NS = not significant using one-way ANOVA followed by Tukey's tests. (C) Double staining with Synapsin-1 and PSD-95. Magnification shows a colocalization between PSD-95 and Synapsin (white arrowhead). Colocalization mask was done using colocalization plug-in from Fiji image software. Bar scale, 20 μm and 10 μm. (D) Representative double staining with NF-M and Olig-2 shown in 3D images acquired by clearing technique from mice with chronic SCI. Dotted line shows the lesion site in vehicle control treatment. White frame magnification in wt-Gal-1 treatment shows regenerated axons with oligodendrocytes in 3D. Bar scale, 250 μm. (E) Bar graph shows the coordinated locomotor recovery quantification. Values represent the mean ± S.D. of five independent experiments (n = 3 mice per group). $^{***}P < 0.0001$ and NS = not significant using one-way ANOVA followed by Tukey's tests. (F) Representative pictures show lack of hindlimb movement in mice treated with vehicle control and the voluntary and coordinated movement in mice traded whit wt-Gal-1 (yellow arrowheads point the hindlimb position in each condition). Bar graph below shows the quantification of foot fall errors. Values represent the mean ± S.D. of five independent experiments (n = 3 mice per group). $^{***}P < 0.0001$ using one-way ANOVA followed by Tukey's tests.

N-glycan-dependent binding of Gal-1 to NRP-1/PlexinA4, which triggered ligand-mediated endocytosis, leaving the neuron surface less sensitive to Sema3A effects. This mechanism might explain the regenerative effects of Gal-1 treatment in damaged axonal tracts leading to recovery of a coordinated locomotor activity in *in vivo* SCI models.

Supplementary data to this article can be found online at http://dx.doi.org/10.1016/j.expneurol.2016.06.009.

Conflict of interest

The authors declare no conflict of interest.

Acknowledgements

We would like to thank James Bamburg and Laurie Minamide (Colorado State University, Colorado, USA) for Lifeact-GFP construct and helpful advice; Jonathan Raper (Department of Neuroscience, Philadelphia, University of Pensilvania, USA) for Sema3A construct. This study was supported by grants from the Argentinian Agency for Promotion of Science and Technology (PICT 2012-0282), to LAP, Argentinian Council of Scientific and Technical Research (PIP-CONICET 11220130100356CO) to JMP and grants from NMSS (RG4530) and Sales Foundation to GAR. CONICYT doctoral fellowship 21120221 to CW and Fondecyt 1140325 and Fondap 15150012 grants to CG-B.

References

Antipenko, A., Himanen, J.P., van Leyen, K., Nardi-Dei, V., Lesniak, J., Barton, W.A., Rajashankar, K.R., Lu, M., Hoemme, C., Puschel, A.W., Nikolov, D.B., 2003. Structure of the semaphorin-3A receptor binding module. Neuron 39, 589–598.

Bareyre, F.M., Kerschensteiner, M., Raineteau, O., Mettenleiter, T.C., Weinmann, O., Schwab, M.E., 2004. The injured spinal cord spontaneously forms a new intraspinal circuit in adult rats. Nat. Neurosci. 7, 269–277.

Belousov, V.V., Fradkov, A.F., Lukyanov, K.A., Staroverov, D.B., Shakhbazov, K.S., Terskikh, A.V., Lukyanov, S., 2006. Genetically encoded fluorescent indicator for intracellular hydrogen peroxide. Nat. Methods 3, 281–286.

Bergeron, Y., Chagniel, L., Bureau, G., Massicotte, G., Cyr, M., 2014. mTOR signaling contributes to motor skill learning in mice. Front. Mol. Neurosci. 7, 26.

Brambilla, R., Hurtado, A., Persaud, T., Esham, K., Pearse, D.D., Oudega, M., Bethea, J.R., 2009. Transgenic inhibition of astroglial NF-kappa B leads to increased axonal sparing and sprouting following spinal cord injury. J. Neurochem. 110, 765–778.

Bregman, B.S., 1987a. Spinal cord transplants permit the growth of serotonergic axons across the site of neonatal spinal cord transection. Brain Res. 431, 265–279.

Bregman, B.S., 1987b. Development of serotonin immunoreactivity in the rat spinal cord and its plasticity after neonatal spinal cord lesions. Brain Res. 431, 245–263.

Chen, J., Wu, J., Apostolova, I., Skup, M., Irintchev, A., Kugler, S., Schachner, M., 2007. Adeno-associated virus-mediated L1 expression promotes functional recovery after spinal cord injury. Brain 130, 954–969.

Cheng, W.Y., Larson, J.M., Samet, J.M., 2014. Monitoring intracellular oxidative events using dynamic spectral unmixing microscopy. Methods 66, 345–352.

Croci, D.O., Cerliani, J.P., Dalotto-Moreno, T., Mendez-Huergo, S.P., Mascanfroni, I.D., Dergan-Dylon, S., Toscano, M.A., Caramelo, J.J., Garcia-Vallejo, J.J., Ouyang, J., Mesri, E.A., Junttila, M.R., Bais, C., Shipp, M.A., Salatino, M., Rabinovich, G.A., 2014. Glycosylation-dependent lectin-receptor interactions preserve angiogenesis in anti-VEGF refractory tumors. Cell 156, 744–758.

De Winter, F., Holtmaat, A.J., Verhaagen, J., 2002a. Neuropilin and class 3 semaphorins in nervous system regeneration. Adv. Exp. Med. Biol. 515, 115–139.

De Winter, F., Oudega, M., Lankhorst, A.J., Hamers, F.P., Blits, B., Ruitenberg, M.J., Pasterkamp, R.J., Gispen, W.H., Verhaagen, J., 2002b. Injury-induced class 3 semaphorin expression in the rat spinal cord. Exp. Neurol. 175, 61–75.

Fan, J., Mansfield, S.G., Redmond, T., Gordon-Weeks, P.R., Raper, J.A., 1993. The organization of F-actin and microtubules in growth cones exposed to a brain-derived collapsing factor. J. Cell Biol. 121, 867–878.

Fournier, A.E., Nakamura, F., Kawamoto, S., Goshima, Y., Kalb, R.G., Strittmatter, S.M., 2000. Semaphorin3A enhances endocytosis at sites of receptor-F-actin colocalization during growth cone collapse. J. Cell Biol. 149, 411–422.

Giridharan, S.S., Caplan, S., 2014. MICAL-family proteins: Complex regulators of the actin cytoskeleton. Antioxid. Redox Signal. 20, 2059–2073.

Goshima, Y., Kawakami, T., Hori, H., Sugiyama, Y., Takasawa, S., Hashimoto, Y., Kagoshima-Maezono, M., Takenaka, T., Misu, Y., Strittmatter, S.M., 1997. A novel action of collapsin: collapsin-1 increases antero- and retrograde axoplasmic transport independently of growth cone collapse. J. Neurobiol. 33, 316–328.

Halpain, S., 2000. Actin and the agile spine: how and why do dendritic spines dance? Trends Neurosci. 23, 141–146.

Hung, R.J., Terman, J.R., 2011. Extracellular inhibitors, repellents, and semaphorin/plexin/MICAL-mediated actin filament disassembly. Cytoskeleton 68, 415–433 (Hoboken).

Hung, R.J., Pak, C.W., Terman, J.R., 2011. Direct redox regulation of F-actin assembly and disassembly by Mical. Science 334, 1710–1713.

Hung, R.J., Yazdani, U., Yoon, J., Wu, H., Yang, T., Gupta, N., Huang, Z., van Berkel, W.J., Terman, J.R., 2010. Mical links semaphorins to F-actin disassembly. Nature 463, 823–827.

Ishikawa-Ankerhold, H.C., Ankerhold, R., Drummen, G.P., 2012. Advanced fluorescence microscopy techniques–FRAP, FLIP, FLAP, FRET and FLIM. Molecules 17, 4047–4132.

Kaech, S., Banker, G., 2006. Culturing hippocampal neurons. Nat. Protoc. 1, 2406–2415.

Kaneko, S., Iwanami, A., Nakamura, M., Kishino, A., Kikuchi, K., Shibata, S., Okano, H.J., Ikegami, T., Moriya, A., Konishi, O., Nakayama, C., Kumagai, K., Kimura, T., Sato, Y., Goshima, Y., Taniguchi, M., Ito, M., He, Z., Toyama, Y., Okano, H., 2006. A selective Sema3A inhibitor enhances regenerative responses and functional recovery of the injured spinal cord. Nat. Med. 12, 1380–1389.

Lee, S.U., Grigorian, A., Pawling, J., Chen, I.J., Gao, G., Mozaffar, T., McKerlie, C., Demetriou, M., 2007. N-glycan processing deficiency promotes spontaneous inflammatory demyelination and neurodegeneration. J. Biol. Chem. 282, 33725–33734.

Limon-Pacheco, J.H., Gonsebatt, M.E., 2010. The glutathione system and its regulation by neurohormone melatonin in the central nervous system. Cent. Nerv. Syst. Agents Med. Chem. 10, 287–297.

Liu, Z., Li, Y., Zhang, J., Elias, S., Chopp, M., 2008. Evaluation of corticospinal axon loss by fluorescent dye tracing in mice with experimental autoimmune encephalomyelitis. J. Neurosci. Methods 167, 191–197.

Liu, K., Lu, Y., Lee, J.K., Samara, R., Willenberg, R., Sears-Kraxberger, I., Tedeschi, A., Park, K.K., Jin, D., Cai, B., Xu, B., Connolly, L., Steward, O., Zheng, B., He, Z., 2010. PTEN deletion enhances the regenerative ability of adult corticospinal neurons. Nat. Neurosci. 13, 1075–1081.

Mann, F., Rougon, G., 2007. Mechanisms of axon guidance: membrane dynamics and axonal transport in semaphorin signalling. J. Neurochem. 102, 316–323.

Marrs, G.S., Green, S.H., Dailey, M.E., 2001. Rapid formation and remodeling of postsynaptic densities in developing dendrites. Nat. Neurosci. 4, 1006–1013.

Matus, A., 2000. Actin-based plasticity in dendritic spines. Science 290, 754–758.

Mendez-Huergo, S.P., Maller, S.M., Farez, M.F., Marino, K., Correale, J., Rabinovich, G.A., 2014. Integration of lectin-glycan recognition systems and immune cell networks in CNS inflammation. Cytokine Growth Factor Rev.

Mire, E., Thomasset, N., Jakeman, L.B., Rougon, G., 2008. Modulating Sema3A signal with a L1 mimetic peptide is not sufficient to promote motor recovery and axon regeneration after spinal cord injury. Mol. Cell. Neurosci. 37, 222–235.

Morinaka, A., Yamada, M., Itofusa, R., Funato, Y., Yoshimura, Y., Nakamura, F., Yoshimura, T., Kaibuchi, K., Goshima, Y., Hoshino, M., Kamiguchi, H., Miki, H., 2011. Thioredoxin mediates oxidation-dependent phosphorylation of CRMP2 and growth cone collapse. Sci. Signal. 4, ra26.

Negishi, M., Oinuma, I., Katoh, H., 2005. Plexins: axon guidance and signal transduction. Cell. Mol. Life Sci. 62, 1363–1371.

Pasquini, L.A., Millet, V., Hoyos, H.C., Giannoni, J.P., Croci, D.O., Marder, M., Liu, F.T., Rabinovich, G.A., Pasquini, J.M., 2011. Galectin-3 drives oligodendrocyte differentiation to control myelin integrity and function. Cell Death Differ. 18, 1746–1756.

Pasterkamp, R.J., Verhaagen, J., 2001. Emerging roles for semaphorins in neural regeneration. Brain Res. Brain Res. Rev. 35, 36–54.

Pasterkamp, R.J., Giger, R.J., Ruitenberg, M.J., Holtmaat, A.J., De Wit, J., De Winter, F., Verhaagen, J., 1999. Expression of the gene encoding the chemorepellent semaphorin III is induced in the fibroblast component of neural scar tissue formed following injuries of adult but not neonatal CNS. Mol. Cell. Neurosci. 13, 143–166.

Quinta, H.R., Galigniana, M.D., 2012. The neuroregenerative mechanism mediated by the Hsp90-binding immunophilin FKBP52 resembles the early steps of neuronal differentiation. Br. J. Pharmacol. 166, 637–649.

Quinta, H.R., Maschi, D., Gomez-Sanchez, C., Piwien-Pilipuk, G., Galigniana, M.D., 2010. Subcellular rearrangement of hsp90-binding immunophilins accompanies neuronal differentiation and neurite outgrowth. J. Neurochem. 115, 716–734.

Quinta, H.R., Pasquini, L.A., Pasquini, J.M., 2015. Three-dimensional reconstruction of corticospinal tract using one-photon confocal microscopy acquisition allows detection of axonal disruption in spinal cord injury. J. Neurochem. 133, 113–124.

Quinta, H.R., Pasquini, J.M., Rabinovich, G.A., Pasquini, L.A., 2014a. Axonal regeneration in spinal cord injury: key role of galectin-1. Medicina 74, 321–325 (B Aires).

Quinta, H.R., Pasquini, J.M., Rabinovich, G.A., Pasquini, L.A., 2014b. Glycan-dependent binding of galectin-1 to neuropilin-1 promotes axonal regeneration after spinal cord injury. Cell Death Differ. 21, 941–955.

Rabinovich, G.A., Croci, D.O., 2012. Regulatory circuits mediated by lectin-glycan interactions in autoimmunity and cancer. Immunity 36, 322–335.

Riedl, J., Crevenna, A.H., Kessenbrock, K., Yu, J.H., Neukirchen, D., Bista, M., Bradke, F., Jenne, D., Holak, T.A., Werb, Z., Sixt, M., Wedlich-Soldner, R., 2008. Lifeact: a versatile marker to visualize F-actin. Nat. Methods 5, 605–607.

Takahashi, T., Fournier, A., Nakamura, F., Wang, L.H., Murakami, Y., Kalb, R.G., Fujisawa, H., Strittmatter, S.M., 1999. Plexin-neuropilin-1 complexes form functional semaphorin-3A receptors. Cell 99, 59–69.

Tamagnone, L., Artigiani, S., Chen, H., He, Z., Ming, G.I., Song, H., Chedotal, A., Winberg, M.L., Goodman, C.S., Poo, M., Tessier-Lavigne, M., Comoglio, P.M., 1999. Plexins are a large family of receptors for transmembrane, secreted, and GPI-anchored semaphorins in vertebrates. Cell 99, 71–80.

Wilson, C., Nunez, M.T., Gonzalez-Billault, C., 2015. Contribution of NADPH-oxidase to the establishment of hippocampal neuronal polarity in culture. J. Cell Sci.

Yang, X., Li, J., Geng, M., 2008. *N*-acetylglucosaminyltransferase V modifies TrKA protein, regulates the receptor function. Cell. Mol. Neurobiol. 28, 663–670.

Zukor, K., Belin, S., Wang, C., Keelan, N., Wang, X., He, Z., 2013. Short hairpin RNA against PTEN enhances regenerative growth of corticospinal tract axons after spinal cord injury. J. Neurosci. 33, 15350–15361.